www.springer.com/41230
https://doi.org/10.1007/s41230-025-4101-6

Effect of La content on microstructure, tensile properties, and electrical conductivity of cast Al-Mg-Si-*x*La alloys

***Hong-yu Xu[1, 2], Hai-feng Jia[2], Ze-sheng Ji[1], Ming-liang Li[1], Han Yu[1], **Bo Jiang[1], Ye Wang[1], and Mao-liang Hu[1]**

1. School of Materials Science and Chemical Engineering, Harbin University of Science and Technology, Harbin 150080, China

2. Weihai Honglin Electronic Co., Ltd., Weihai 264205, Shandong, China

Abstract: Lightweight aluminum alloy conductor materials (Al-Mg-Si alloys) require not only high electrical conductivity to reduce electrical loss, but also high strength to withstand extreme weather conditions. To improve electrical conductivity and mechanical properties of Al-Mg-Si alloy simultaneously, the rare earth La was introduced to modify the Al-Mg-Si alloy. The effect of La addition on the microstructure, tensile properties and electrical conductivity of cast Al-Mg-Si alloy was investigated systematically. Results indicate that the appropriate La content is helpful to improve the strength and electrical conductivity of Al-Mg-Si alloys. When the addition of La is 0.2wt.%, the α-Al grains are refined apparently, Mg and Si solute atoms in the Al matrix are reduced by the formation of Mg_2Si phase; the distribution of $Al_{11}La_3$ phases is uniform, and the morphology of AlFeSi phase transforms from continuous state to discontinuous state. The Al-Mg-Si-0.2La alloy exhibits the optimal tensile properties and electrical conductivity, with an ultimate tensile strength of 170 MPa, a yield strength of 88 MPa, an elongation of 18.9%, and an electrical conductivity of 44.0% IACS. These values represent improvements of 9.0%, 15.8%, 70.3%, and 17.3%, respectively, compared to the Al-Mg-Si alloy without La addition. However, excessive La deteriorates the properties of Al-Mg-Si-*x*La alloys.

Keywords: Al-Mg-Si alloy; rare earth La; microstructure; tensile properties; electrical conductivity

CLC numbers: TG146.21 **Document code:** A **Article ID:** 1672-6421(2025)04-385-10

1 Introduction

With the construction of a new type of power system and the transition of clean and low-carbon energy, there is an urgent requirement for lightweight aluminum and aluminum alloy conductor materials with excellent comprehensive properties. For example, aluminum alloy conductor materials require not only high conductivity to reduce electrical loss rates, but also high strength to effectively withstand extreme weather conditions [1]. Compared with pure aluminum, the strength of Al-Mg-Si alloy (a typical conductor material) is significantly enhanced, but the electrical conductivity is decreased seriously [2-5]. The contradiction between electrical conductivity and strength is the key problem that limits its wide application. In general, the electrical conductivity of alloy is very sensitive to the solute atoms, which usually intensify the electron scattering, therefore, leading to a reduction in conductivity [6-9].

To increase strength and electrical conductivity of Al-Mg-Si alloys, researchers have made a lot of efforts [10-12]. Karabay [10] designed a modification method, combining the AlB_2 addition with artificial aging treatment, to promote the concurrent enhancements of the strength and electrical conductivity of 6201 alloy. Khangholi et al. [11] proposed a strategy for manufacturing Al-Mg-Si alloy, with a superior strength of 369 MPa and an acceptable conductivity of 53% IACS, by combining the natural aging with pre-aging treatment. Zheng et al. [12] found that it is a feasible method to improve the mechanical properties and electrical conductivity of Al-Mg-Si alloys by combining trace Ca, Mn addition with solution and

***Hong-yu Xu**

Ph. D., Associate Professor. His research interests mainly focus on the rare earth aluminum alloy, aluminum/magnesium matrix composite. To date, he has published about 40 papers and received two Science and Technology Awards from Heilongjiang Province for his distinguished research.

E-mail: xuhongyu@hrbust.edu.cn

****Bo Jiang**

E-mail: jiangbo@hrbust.edu.cn

Received: 2024-05-20; Revised: 2024-09-12; Accepted: 2024-12-12

aging treatment. According to these studies, the improvement of electrical conductivity of Al-Mg-Si alloy mainly relies on subsequent heat treatment, while the mechanical properties of cast Al-Mg-Si alloy enhance at the expense of electrical conductivity [13].

Rare earth alloying is an effective method to improve the solidification structure and properties of alloy. In recent years, the use of rare earth to regulate the microstructure and properties of aluminum alloys has been widely concerned [13-20]. It is indicated that rare earth elements have significant potential in improving the microstructure and properties of alloys, although previous studies have shown inconsistencies. Zhao et al. [18] added La into Al-0.5Mg-0.24Si alloy to form the $LaSi_2$ phase, which promoted the transformation of the Fe-rich phase from β-Al_5FeSi to α-Al_8Fe_2Si, and the appropriate La content improved the tensile properties and electrical conductivity of the alloy. However, Medvedev et al. [19] found that the conductivity of aluminum alloy with addition of rare earth Ce and La was reduced due to its partial dissolution into the Al matrix. Jiang et al. [20] adopted trace La to reduce the grain size of Al-Mg-Si alloys and promote the precipitation of Mg_2Si phases, which improved the tensile strength of the alloys from 310 MPa to 361 MPa. Nonetheless, Ding et al. [21] reported that the addition of rare earth Y decreased the tensile strength of Al-Cu-Mg-Ag alloy. The controversial results demonstrate that the effect of rear earth on the microstructure and properties of the Al-Mg-Si alloy needs to be further studied.

In this study, the enhancement of both strength and electrical conductivity in cast Al-Mg-Si alloy through the addition of rare earth La was proposed. The effects of La addition on the microstructure, tensile properties, and electrical conductivity of the cast Al-Mg-Si alloy were systematically investigated. Additionally, the influence mechanisms of La were analyzed in detail. This research may serve as a reference for the preparation of Al-Mg-Si alloys with excellent mechanical properties and electrical conductivity.

2 Experimental procedure

Al-Mg-Si-*x*La alloys (*x*=0, 0.1, 0.2, 0.3, 0.4, 0.5, in wt.%) were prepared from pure aluminum (99.9%), pure magnesium (99.9%), Al-20Si and Al-20La master alloys, and the specific chemical compositions are shown in Table 1. The detailed melting process was as follows: Firstly, a certain amount of pure aluminum and Al-20Si master alloy were put into a graphite crucible and melted in a resistance furnace. When they were completely melted at 750 °C, the pure magnesium wrapped in aluminum foil and Al-20La master alloy were added into the melt by using of a bell jar and stirred for 5 min. Then, the refining agent was added and stirred to remove the slags and gases, and the melt was holding for 10 min. Finally, the melt was cooled down to 720 °C and poured into the preheated metal mold to obtain the Al-Mg-Si-*x*La alloy ingots.

Al-Mg-Si-*x*La alloy samples for microstructure observation were ground, polished, and then etched using a 1% hydrofluoric acid solution. The metallographic samples were treated in a 4% fluoroborate solution for 90 s to obtain anodic coating, and then were observed under polarized light. Microstructure observation of the alloys was conducted by using an optical microscope (OM, Leica DM ILM) and a scanning electron microscope (SEM, FEI Sirion 200). The phase constitution was analyzed using an X-ray diffractometer (XRD, X'Pert Pro) with a scanning speed of 9°·min^{-1} and a scanning angle of 10°–90°. The phase in the alloys was characterized by a transmission electron microscope (TEM, JEM-2100). The tensile properties of the alloys were tested on an Instron 569/50 K universal tensile testing machine at room temperature, under a loading speed of 1 mm·min^{-1}. The geometry and sizes of the tensile test samples are shown in Fig. 1. The electrical conductivity of the alloys was measured using an RTS-11 metal four-probe tester. The conductivity test sample is shown in Fig. 2. The melting behaviors of the Al-Mg-Si-*x*La alloys under an argon atmosphere were studied using differential scanning calorimetry (DSC), employing a Netzsch STA 449 F5 model. The samples were heated from 25 °C to 750 °C with a heating rate of 5 K·min^{-1}.

Table 1: Chemical compositions of Al-Mg-Si-*x*La alloys (wt.%)

Alloys	Mg	Si	Fe	La	Al
Al-Mg-Si	0.71	0.66	0.48	0.00	Bal.
Al-Mg-Si-0.1La	0.70	0.67	0.47	0.11	Bal.
Al-Mg-Si-0.2La	0.71	0.67	0.46	0.19	Bal.
Al-Mg-Si-0.3La	0.71	0.67	0.46	0.28	Bal.
Al-Mg-Si-0.4La	0.69	0.67	0.47	0.41	Bal.
Al-Mg-Si-0.5La	0.71	0.67	0.46	0.53	Bal.

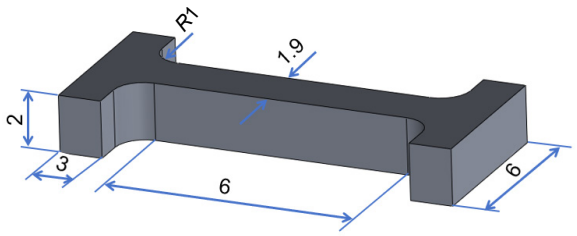

Fig. 1: Geometry and sizes of tensile specimen (units: mm)

Fig. 2: Geometry and sizes of conductive sample (units: mm)

3 Results and discussion

3.1 Microstructure of cast Al-Mg-Si-*x*La alloys

Figure 3 presents the OM images of Al-Mg-Si-*x*La alloys. The corresponding area fraction of the second phase is listed in Table 2. It can be observed that the Al-Mg-Si alloy contains coarse, dark gray phases with irregular needle-like and bone-like shapes that continuously distribute along the grain boundaries, though the majority exhibit a needle-like morphology, as shown in Fig. 3(a). In addition, a few black spherical phases are dispersed in the Al matrix. After La is added, the second phases in the Al-Mg-Si-*x*La alloys are mainly in needle-like shape. Notably, when the La content is below 0.2wt.%, the size of these second phases is significantly reduced, and their quantity also decreases markedly. However, as the content of La continues to rise, the amounts of the second phases experience an increase instead. Nevertheless, the trend in this regard is not particularly evident. Moreover, the number of the black spherical phase continuously increases from 0.63% to 1.20%.

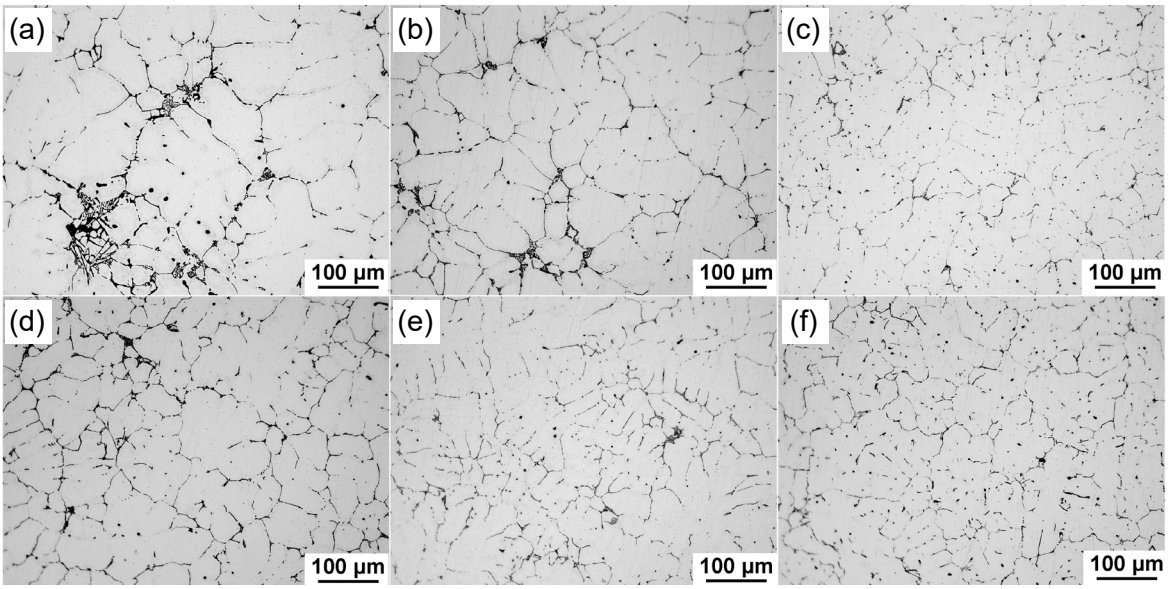

Fig. 3: OM images of Al-Mg-Si-*x*La alloys: (a) Al-Mg-Si; (b) Al-Mg-Si-0.1La; (c) Al-Mg-Si-0.2La; (d) Al-Mg-Si-0.3La; (e) Al-Mg-Si-0.4La; (f) Al-Mg-Si-0.5La

Table 2: Area fraction of the second phase of Al-Mg-Si-*x*La alloys (%)

Second phase	Al-Mg-Si	Al-Mg-Si-0.1La	Al-Mg-Si-0.2La	Al-Mg-Si-0.3La	Al-Mg-Si-0.4La	Al-Mg-Si-0.5La
Needle-like phase	3.11%	2.89%	1.53%	3.29%	2.46%	3.19%
Bone-like phase	1.11%	0.93%	0.21%	1.03%	0.67%	1.02%
Black spherical phase	0.63%	0.66%	1.03%	1.04%	1.07%	1.20%

The polarized light morphologies and the distributions of the grain size of Al-Mg-Si-*x*La alloys are shown in Fig. 4. The calculation results show that the average grain size of the Al-Mg-Si-*x*La alloys is about 271.9 μm, 201.6 μm, 141.7 μm, 146.8 μm, 175.5 μm, and 180.1 μm, respectively, as La addition amount increases from 0 to 0.5wt.%. It can be seen that the grains of the Al-Mg-Si alloy are refined after the addition of La. The grain refinement effect of the Al-Mg-Si-0.2La alloy is the optimal and the average grain size is reduced by about 47.9% compared with that of the Al-Mg-Si alloy. When the La content exceeds 0.2wt.%, the average grain size of the alloys gradually increases. Furthermore, after adding La, the distribution of the grain size is more uniform in the Al-Mg-Si-*x*La alloys, as shown in Fig. 4(a_1)-(f_1).

Generally, rare earth La refines α-Al primarily through the following mechanisms: (1) promoting the formation of nucleation sites; (2) restraining the growth of α-Al; (3) reducing the wetting angle θ between the nucleation sites and α-Al [22, 23]. Studies indicate that La can form $Al_{11}La_3$ and AlFeLa phases in aluminum alloys [24, 25], which facilitates the creation of α-Al nucleation sites upon the addition of La.

It is difficult for La atoms to be dissolved in α-Al due to the fact that the atomic radius of La is much greater than that of Al and the misfit degree of La and Al is about 59at.% [26, 27]. During the solidification process, La is ejected from α-Al and then enriched in the solidification interface during the growth of α-Al, which can restrain the growth of α-Al grains. The growth restriction factor (GRF) is used to reflect the effect of La elemental enrichment on grain refinement, expressed as follows [28]:

$$\mathrm{GRF} = C_{\mathrm{La}} m\,(k-1) \quad (1)$$

where C_{La} is the concentration of La element in the Al-Mg-Si alloy, m = –2.034 is the slope of the liquid-phase line of the Al-La alloy, and k=0.003 is the equilibrium distribution coefficient of

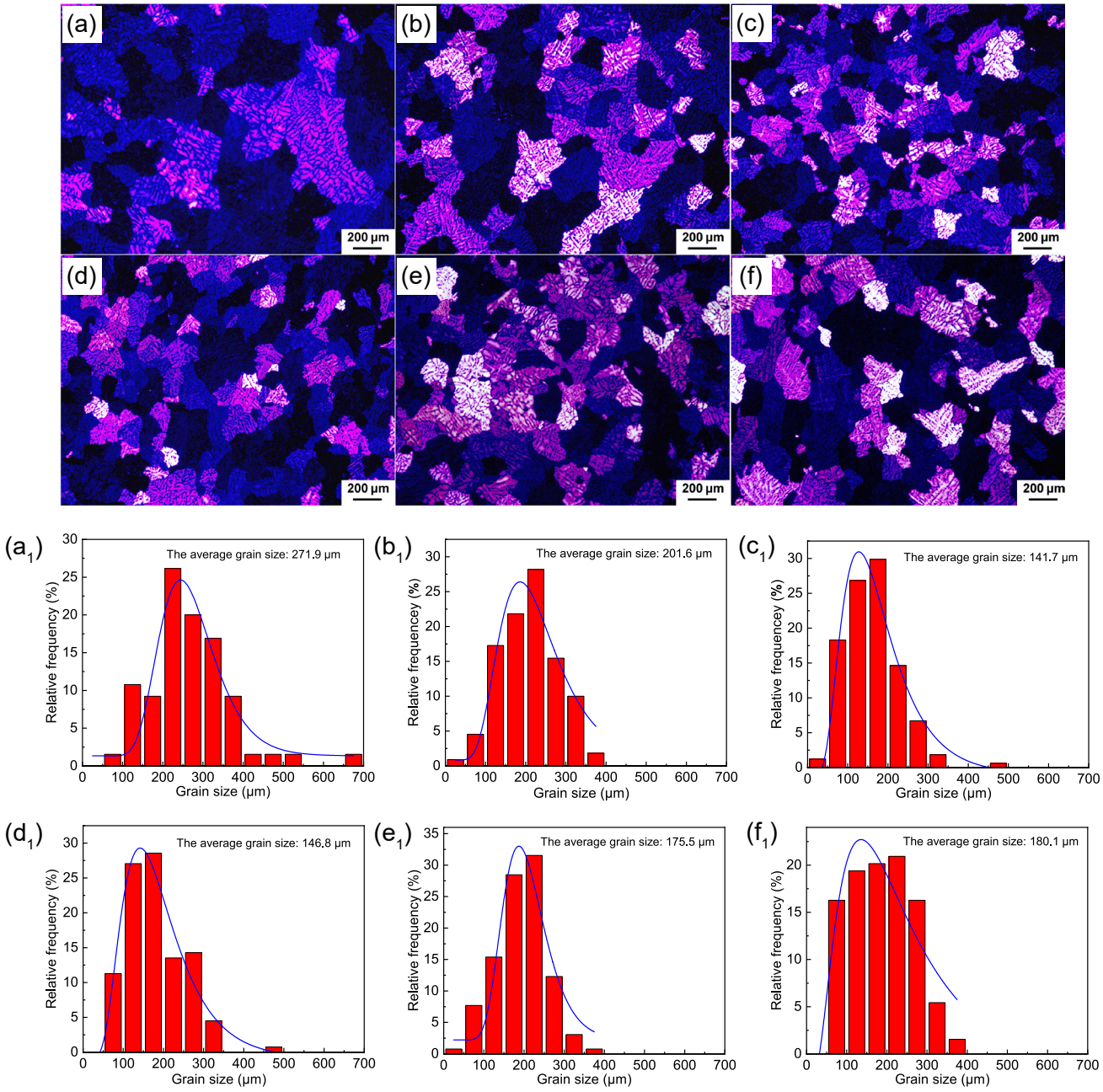

Fig. 4: Polarized light morphologies and distributions of the corresponding grain size of Al-Mg-Si-*x*La alloys: (a, a_1) Al-Mg-Si; (b, b_1) Al-Mg-Si-0.1La; (c, c_1) Al-Mg-Si-0.2La; (d, d_1) Al-Mg-Si-0.3La; (e, e_1) Al-Mg-Si-0.4La; (f, f_1) Al-Mg-Si-0.5La

La element in the Al-La alloy [23, 29]. The increment of GRF is calculated to be approximately 0.20 K to 1.01 K by adding 0.1wt.% to 0.5wt.% La. This demonstrates that the La addition has little effect on restraining the growth of α-Al.

The liquidus temperature of the Al-Mg-Si alloy calculated by JMatPro software is 652.0 °C. Figure 5 shows the DSC curves of cast Al-Mg-Si and Al-Mg-Si-0.2La alloys. The nucleation undercooling of α-Al nucleus for Al-Mg-Si alloy is about 8.3 °C and that of α-Al nucleus for Al-Mg-Si-0.2La alloy is about 3.6 °C. Both of them are much less than 0.2 T_m (T_m is the liquidus temperature, K), indicating that the growth of α-Al nucleus is based on heterogeneous nucleation in the solidification [23]. According to the theory of heterogeneous nucleation, the wetting angle θ plays a crucial role. Research has shown that La can promote grain size reduction by decreasing the wetting angle [26]. The wetting angle θ is calculated as follows [23]:

$$f(\theta)=\left(2-3\cos\theta+\cos^3\theta\right)/4=27\left(\Delta T^{\alpha-\mathrm{Al}}\right)^2\Delta T_{\mathrm{N}}^{\alpha-\mathrm{Al}}/4\left(\Delta T_{\mathrm{L}}^{\alpha-\mathrm{Al}}\right)^3 \quad (2)$$

where $\Delta T^{\alpha-\mathrm{Al}}$ is the nucleation undercooling (K) of α-Al, $\Delta T_{\mathrm{N}}^{\alpha-\mathrm{Al}}$ is the nucleation temperature (K) of α-Al and $\Delta T_{\mathrm{L}}^{\alpha-\mathrm{Al}}$ is the liquidus temperature (K) of the alloys. According to the calculation, the value of wetting angle θ for Al-Mg-Si alloy is 13.3° and it decreases to 8.8° for Al-Mg-Si-0.2La alloy. Therefore, the addition of La can promote the refinement of grains in Al-Mg-Si alloy by decreasing the wetting angle. This is consistent with the relevant research results [20].

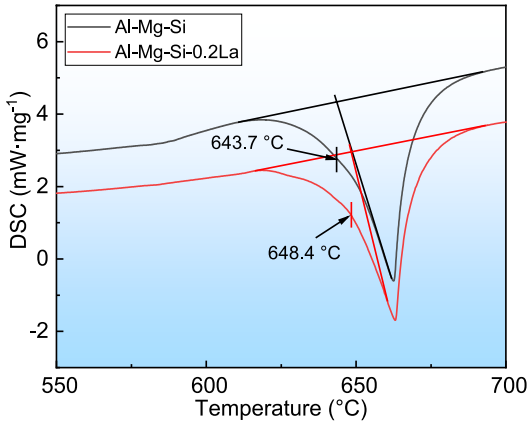

Fig. 5: DSC curves of Al-Mg-Si and Al-Mg-Si-0.2La alloys

3.2 Effect of La on second phase

The XRD patterns of Al-Mg-Si-*x*La alloys are shown in Fig. 6. The analysis results indicate that the cast Al-Mg-Si alloy mainly consists of α-Al, Mg_2Si, and β-AlFeSi phases. The diffraction peaks of the $Al_{11}La_3$ phase appear after the addition of La, and their intensity has no evident changes with the increase of La content. In addition, compared to the Al-Mg-Si alloy, the intensity of diffraction peaks of the Mg_2Si phase slightly increases after adding La. It suggests that the addition of La can promote the formation of the Mg_2Si phase, which is consistent with the results in Fig. 3, and the same conclusion is also found in the Li's work [30].

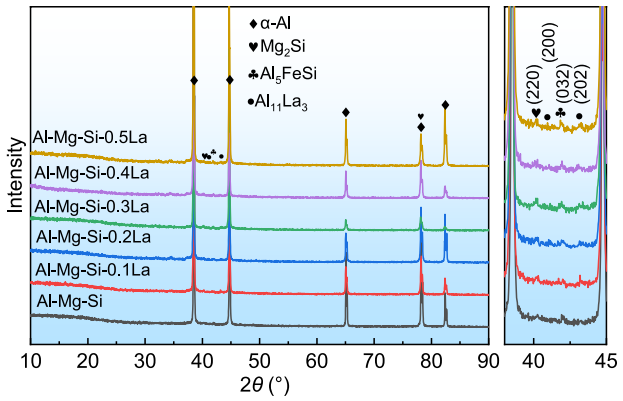

Fig. 6: XRD patterns of Al-Mg-Si-*x*La alloys

The SEM microstructure and EDS mappings of Al-Mg-Si-*x*La alloys are presented in Fig. 7. It can be observed that the point-like and needle-like rare earth phases appear in the Al-Mg-Si-*x*La alloys after adding La. When the La content is less than 0.2wt.%, the rare earth phase mainly exists in the point-like shape. However, when the La content exceeds 0.2wt.%, the presence of needle-like rare earth phases increases significantly. Moreover, the Mg_2Si phase, which is mainly distributed at the grain boundaries, also increases significantly in the Al-Mg-Si-*x*La alloys. However, as the La content exceeds 0.2wt.%, the number of Mg_2Si phase does not continue to increase. This observation aligns with relevant literature, indicating that trace amounts of La can facilitate the formation of Mg_2Si particles during solidification [31].

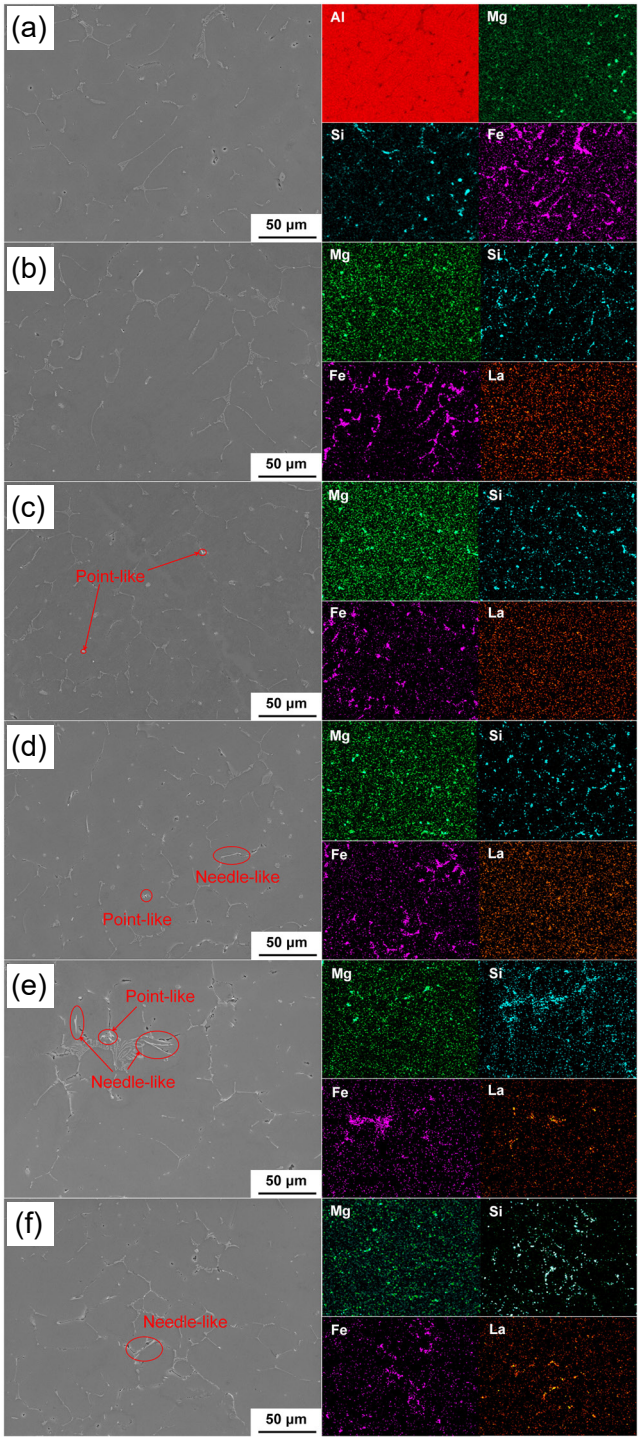

Fig. 7: SEM microstructures and EDS mappings of Al-Mg-Si-*x*La alloys: (a) Al-Mg-Si; (b) Al-Mg-Si-0.1La; (c) Al-Mg-Si-0.2La; (d) Al-Mg-Si-0.3La; (e) Al-Mg-Si-0.4La; (f) Al-Mg-Si-0.5La

Figure 8 shows the SEM images of Al-Mg-Si alloy and Al-Mg-Si-0.3La alloy, and the chemical compositions of the corresponding points determined by EDS are listed in Table 3. In general, most of the Fe-containing phases present in cast Al-Mg-Si alloy are β-AlFeSi phase (Al_5FeSi) and α-AlFeSi phase (Al_8Fe_2Si). The values of Fe and Si atomic ratio of Al_5FeSi phase and Al_8Fe_2Si phase are 1 to 1.3 and 1.5 to 2, respectively [32, 33]. Figures 8(a) and (b) exhibit the bone-like and needle-like AlFeSi phases in cast Al-Mg-Si alloy, respectively. The value of the

Fe and Si atomic ratio is about 1.70 for the bone-like phase, and about 0.89 for the needle-like phase. Therefore, combined with XRD pattern in Fig. 6 and Table 3, it can be determined that the bone-like AlFeSi phase is Al_8Fe_2Si and the needle-like AlFeSi phase is Al_5FeSi. Figures 8(c) and (d) show the bone-like and needle-like phases of cast Al-Mg-Si-0.3La alloy, respectively. After adding La, the value of the Fe and Si atomic ratio of the bone-like Al_8Fe_2Si phase is about 1.67, and that of the needle-like Al_5FeSi phase is about 0.95.

Additionally, it is observed in Fig. 8 that the morphology of the AlFeSi phase transitions from a continuous state to a discontinuous state following the addition of La. It has been suggested that rare earth La promotes the transformation of the β-AlFeSi phase to the α-AlFeSi phase [34], but no such transformation is found in this study.

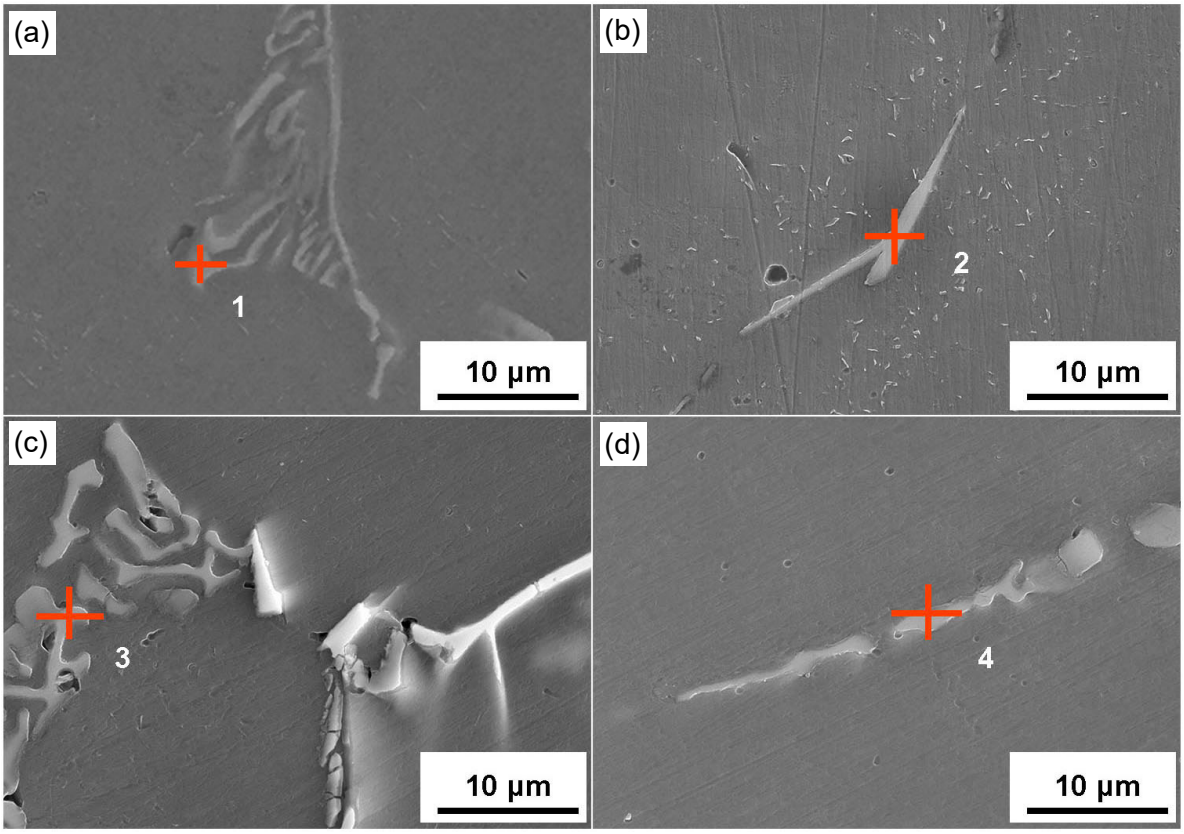

Fig. 8: SEM images of Al-Mg-Si alloy and Al-Mg-Si-0.3La alloy: (a, b) Al-Mg-Si alloy; (c, d) Al-Mg-Si-0.3La alloy

Table 3: EDS results of the corresponding points in Fig. 8

Point No.	Atomic fraction (%)				
	Al	Mg	Si	Fe	Fe/Si
1	89.48	0.50	3.71	6.31	1.70
2	85.10	0.73	7.51	6.66	0.89
3	84.61	2.17	4.92	8.30	1.67
4	84.51	4.17	5.82	5.50	0.95

The SEM and the corresponding EDS images of the rare earth phase in Al-Mg-Si-0.4La alloy are shown in Fig. 9. It is observed that a portion of the La-rich phase exhibits a needle-like morphology, while another portion presents a point-like appearance. Both morphologies are distributed along the grain boundaries of the Al-Mg-Si alloys. The results of EDS reveal that both of the point-like phase and needle-like phase mainly consist of Al, Mg, Si, and La elements, and they are free of Fe elements. It is noteworthy that the Mg_2Si phases are mainly distributed around the La-rich rare earth phase according to the distribution of the elements shown in Fig. 9. La readily combines with Al to form new phases in the Al-Mg-Si-*x*La alloys [35, 36]. Additionally, the rare earth phase can nucleate and grow on the surface of the Mg_2Si phase [23]. Therefore, it is speculated that the La-rich phase in the Al-Mg-Si-*x*La alloys is an Al-La binary phase.

Furthermore, the TEM analysis was used to verify the above speculation. Figure 10 shows the TEM images of the needle-like rare earth phase. The rare earth phase exhibits a face-centered cubic structure by calibrating the diffraction spots, as shown in Fig. 10(c). Through the inverse fast Fourier transformation (IFFT), the interplanar spacing of the (002) crystalline plane is obtained to be 0.6449 nm in the high-resolution image [Fig. 10(d)], which is close to that of $Al_{11}La_3$ phase [37]. Therefore, it is determined that the needle-like rare earth phase is the $Al_{11}La_3$ phase. This is consistent with the results of XRD.

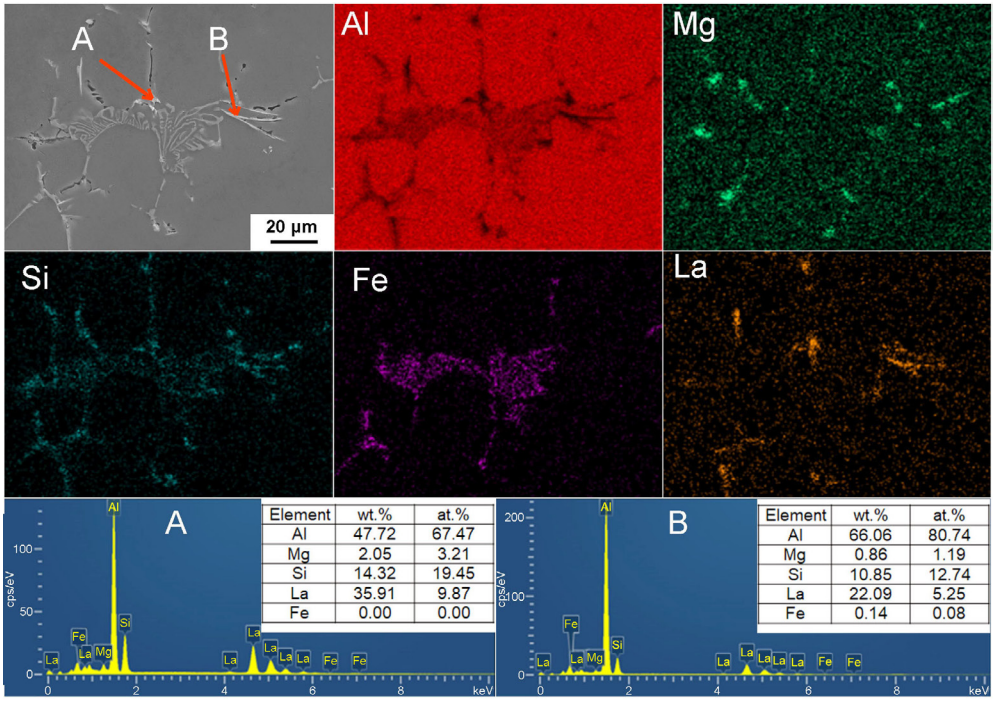

Fig. 9: SEM and the corresponding EDS images of rare earth phases in Al-Mg-Si-0.4La alloy

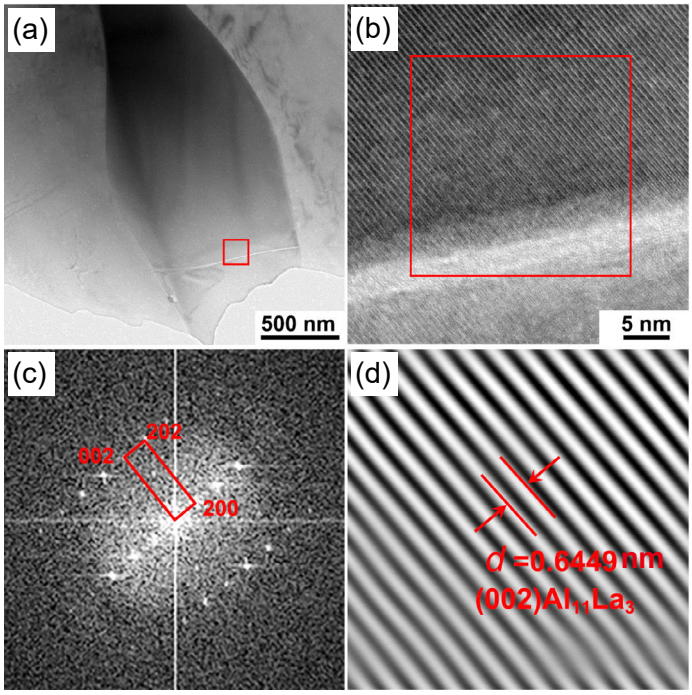

Fig. 10: TEM images of rare earth phase: (a) bright field image of rare earth phase; (b) the corresponding HRTEM image; (c) the corresponding FFT pattern; (d) the corresponding IFFT pattern

3.3 Tensile properties

Figure 11 shows the engineering stress-strain curves and the tensile properties of the cast Al-Mg-Si-*x*La alloys. The ultimate tensile strength (UTS), yield strength (YS), and elongation (EL) of Al-Mg-Si-*x*La alloys present a tendency of initially increase and subsequently decrease with an increase in La content. Compared with the Al-Mg-Si alloy (UTS: 156 MPa, YS: 76 MPa, and EL: 11.1%), the Al-Mg-Si-0.2La alloy exhibits the optimal tensile properties with UTS of 170 MPa, YS of 88 MPa, and EL of 18.9%, which are improved by 9.0%, 15.8%, and 70.3%, respectively. However, the tensile properties of the Al-Mg-Si-*x*La alloys gradually decrease when the content of La exceeds 0.2wt.%.

The tensile fracture morphologies of the Al-Mg-Si-*x*La alloys are shown in Fig. 12. On the whole, the fracture surfaces of Al-Mg-Si-*x*La alloys are mainly composed of dimples and small cleavage planes, which is clearly characterized by ductile fracture. There are many large dimples, a few cleavage planes, and a small number of microcracks at the fracture surface of Al-Mg-Si alloy, as shown in Fig. 12(a). After adding

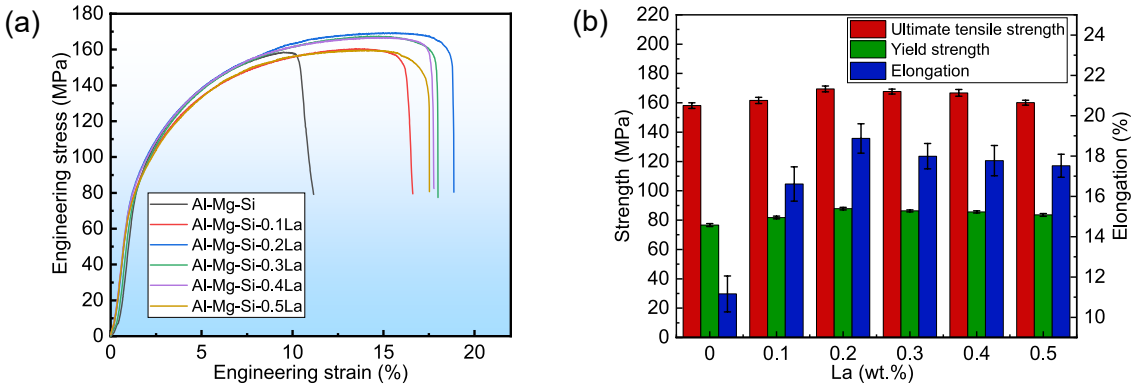

Fig. 11: Tensile properties of Al-Mg-Si-*x*La alloys: (a) engineering stress-strain curves; (b) tensile strength and elongation

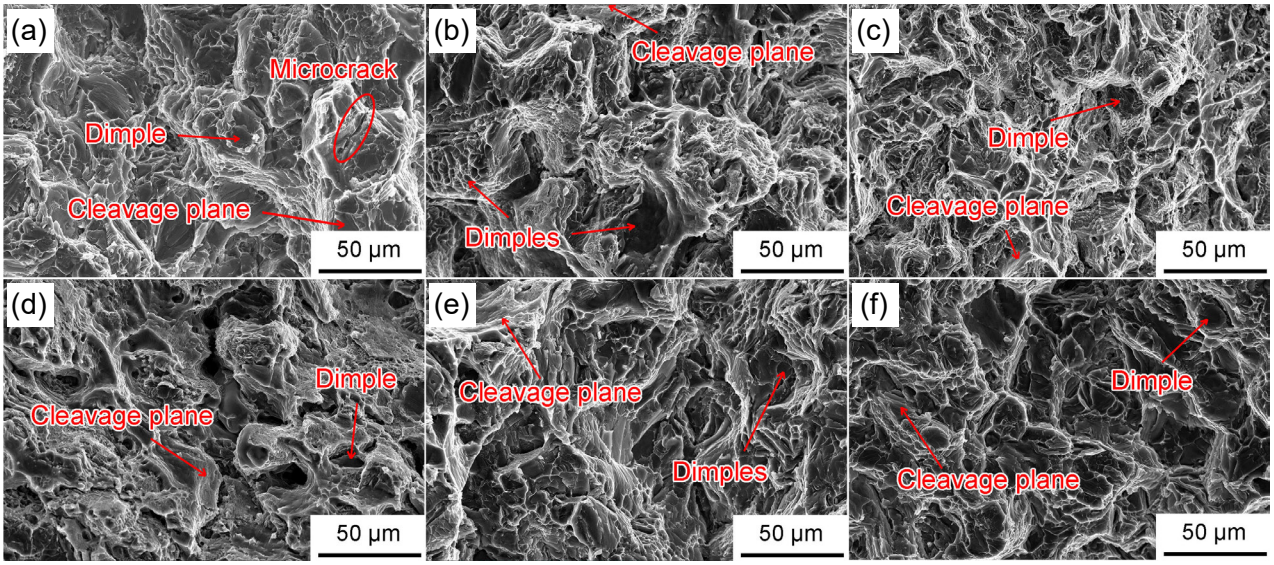

Fig. 12: Fracture surface morphologies of Al-Mg-Si-*x*La alloys: (a) Al-Mg-Si; (b) Al-Mg-Si-0.1La; (c) Al-Mg-Si-0.2La; (d) Al-Mg-Si-0.3La; (e) Al-Mg-Si-0.4La; (f) Al-Mg-Si-0.5La

La, the microcracks basically disappear, and the dimples firstly increase and then decrease while the cleavage planes show the opposite trend with the increase of La content, as shown in Figs. 12(b)–(f). Moreover, when La content is 0.2wt.%, the dimples of consistent size are uniformly distributed at the fracture surface of Al-Mg-Si-0.2La alloy, accompanied by a scarcity of cleavage planes. However, when the La content exceeds 0.2wt.%, the number of dimples reduces gradually, but the cleavage planes are more obvious.

Combined with the microstructure analysis, the strengthening effect of La in the Al-Mg-Si-*x*La alloys is mainly attributed to fine grain strengthening and second phase strengthening. When the addition content of La is 0.2wt.%, the average grain size is the smallest, which enhances the tensile properties of the Al-Mg-Si-0.2La alloy. The increase of the Mg_2Si phase and a small amount of the point-like $Al_{11}La_3$ phases are also beneficial for the tensile properties of the Al-Mg-Si-0.2La alloy. Furthermore, the change of the AlFeSi phase morphology from continuous state to discontinuous state has a positive effect on the tensile properties of the Al-Mg-Si-0.2La alloy. When the addition content of La is more than 0.2wt.%, the increase of Mg_2Si phase is not obvious. However, the average grain size of the Al-Mg-Si-*x*La alloys gradually increases. Furthermore, many needle-like $Al_{11}La_3$ phases are formed in the Al-Mg-Si-*x*La alloys, which is detrimental to the tensile properties of the Al-Mg-Si-*x*La alloys. As a result, the tensile properties of the Al-Mg-Si-*x*La alloys gradually decrease when the La content exceeds 0.2wt.%.

3.4 Electrical conductivity

Figure 13 presents the variation curves of electrical conductivity of the cast Al-Mg-Si-*x*La alloys. The electrical conductivities of the cast Al-Mg-Si-*x*La alloys are 37.5%, 43.4%, 44.0%, 42.8%, 42.5%, and 41.6% IACS, respectively, which also increase at first and then decrease with an increase in La content from 0 to 0.5wt.%. It is observed that La can significantly improve the electrical conductivity of the cast Al-Mg-Si-*x*La alloys. When the La addition is 0.2wt.%, the electrical conductivity of the Al-Mg-Si-0.2La alloy achieves the maximum value, which is about 17.3% higher than that of the Al-Mg-Si alloy. When the La content exceeds 0.2wt.%, the electrical conductivity declines gradually, and it decreases to 41.6% IACS of Al-Mg-Si-0.5La alloy, which is still 10.9% higher than that of the Al-Mg-Si alloy.

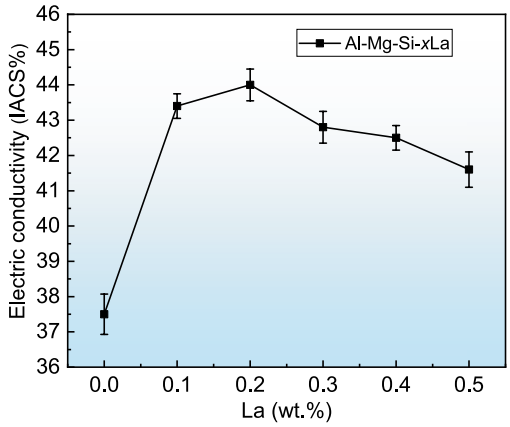

Fig. 13: Variation curve of electrical conductivity of Al-Mg-Si-*x*La alloys

According to the Matthiessen's rule, the total resistivity of the alloy could be expressed as follows [38]:

$$\rho_d = \rho_{ss} + \rho_p + \rho_{dis} + \rho_{gb} \quad (3)$$

where ρ_d is the resistance caused by crystal defects of the alloy, ρ_{ss}, ρ_p, ρ_{dis}, and ρ_{gb} are the resistance caused by solid solution atoms, phases, dislocations, and grain boundaries, respectively. The dislocation of cast Al-Mg-Si-*x*La alloys can be neglected in this study. Based on the above analysis of the microstructure, the effect of La on the electrical conductivity of the Al-Mg-Si-*x*La alloys is mainly due to the decrease of solute atoms, the increase of grain boundaries, and the change of second phase morphology.

According to the theory of electrical conductivity of metals, the solid solution atom is the most influential factor on the electrical conductivity of the metal, followed by defects, the grain boundaries, and the second phases [39]. Firstly, the Mg_2Si phase significantly increase in the Al-Mg-Si-*x*La alloys as the La content increases from 0 to 0.2wt.%. This indicates that Mg and Si solute atoms in the Al matrix are obviously reduced by the formation of Mg_2Si phase, which will remarkably increase the electron transport efficiency of the alloy. Then, the number of grain boundaries increases due to the grain refinement of cast Al-Mg-Si-*x*La alloys, and the homogeneity of Al matrix is improved, resulting in the reduction of scattering ability of structural stress on electrons. At last, the transformation of the AlFeSi phase morphology from a continuous to a discontinuous state, along with the presence of point-like $Al_{11}La_3$ particles, exerts a beneficial influence on the electrical conductivity of the alloys. Therefore, the Al-Mg-Si-0.2La alloy exhibits the optimal electrical conductivity.

However, when the La content exceeds 0.2wt.%, the precipitation of Mg and Si solute atoms from the Al matrix is obviously weakened, and many needle-like $Al_{11}La_3$ phases form due to the segregation of excessive La, enhancing the scattering of electrons. Thus, the electrical conductivity of the Al-Mg-Si-*x*La alloys gradually degrades. In addition, La also can remove the gas (H_2) and the slag (Al_2O_3) during the melting process, which may be one of the reasons why the electrical conductivity of the Al-Mg-Si-*x*La alloys is still better than that of the Al-Mg-Si alloy.

4 Conclusions

The effects of La content on the microstructure evolution, tensile properties, and electrical conductivity of cast Al-Mg-Si-*x*La alloys were studied in detail. The main conclusions are drawn as follows:

(1) La can refine the grains of the cast Al-Mg-Si-*x*La alloys by reducing the wetting angle. At the optimal La content of 0.2wt.%, the average grain size of the Al-Mg-Si-0.2La alloy is reduced by 47.9% compared with that of the Al-Mg-Si alloy.

(2) La promotes the formation of the Mg_2Si phase and induces a morphological transformation in the AlFeSi phase, transitioning it from a continuous to a discontinuous state. However, excessive La will form many needle-like $Al_{11}La_3$ phases.

(3) The Al-Mg-Si-0.2La alloy exhibits the optimal tensile properties and electrical conductivity with an ultimate tensile strength of 170 MPa, a yield strength of 88 MPa, an elongation of 18.9%, and an electrical conductivity of 44.0% IACS, which are 9.0%, 15.8%, 70.3%, and 17.3% higher than that of the Al-Mg-Si alloy, respectively.

(4) The enhancement of tensile properties of Al-Mg-Si-0.2La alloy is mainly attributed to the fine grain strengthening and the second phase strengthening. Furthermore, the improvement of electrical conductivity is mainly ascribed to the lower Mg and Si solute atoms in the Al-Mg-Si-0.2La alloy.

Acknowledgments

This work was financially supported by the National Natural Science Foundation of China (No. 51704087) and the Natural Science Foundation of Heilongjiang Province (No. LH2020E083).

Conflict of interest

The authors declare that they have no known competing financial interests or personal relationships that could have appeared to influence the work reported in this paper.

References

[1] Fan G, Feng Y T, Geng J H, et al. Electric energy loss property and energy saving effect of energy saving wire. Electrical Engineering Materials, 2016, 3: 20–24.
[2] Gursoy O, Timelli G. Lanthanides: A focused review of eutectic modification in hypoeutectic Al-Si alloys. Journal of Materials Research and Technology, 2020, 9(4): 8652–8666.
[3] Zheng Y Y, Luo B H, Xie W, et al. Microstructure evolution and precipitation behavior of Al-Mg-Si alloy during initial aging. China Foundry, 2023, 20(1): 57–62.
[4] Meng F B, Huang H J, Yuan X G, et al. Segregation in squeeze casting 6061 aluminum alloy wheel spokes and its formation mechanism. China Foundry, 2021, 18(1): 45–51.
[5] He C, Li Y, Li J D, et al. Effect of electromagnetic fields on microstructure and tensile properties of sub-rapid solidification-processed Al-Mg-Si alloy during twin-roll casting. Materials Science and Engineering: A, 2019, 766: 138328.

[6] Siamak N K, Mousa J, Alexandre M, et al. Optimization of tensile properties and electrical conductivity in Al-Mg-Si 6201 alloys with different Mg/Si ratios. Journal of Materials Research, 2020, 35(20): 2765–2776.
[7] Fu J N, Yang Z, Deng Y L, et al. Influence of Zr addition on precipitation evolution and performance of Al-Mg-Si alloy conductor. Materials Characterization, 2020, 159: 110021.
[8] Chen Z G, Yang W L, Wang S Y, et al. Research progress of microalloyed Al alloys. Rare Metal Materials and Engineering, 2010, 39(8): 1499–1504.
[9] Jiang S Y, Wang R H. Grain size-dependent Mg/Si ratio effect on the microstructure and tensile/electrical properties of Al-Mg-Si-Sc alloys. Journal of Materials Science Technology, 2019, 35(7): 1354–1363.
[10] Karabay S. Modification of AA-6201 alloy for manufacturing of high conductivity and extra high conductivity wires with property of high tensile stress after artificial aging heat treatment for all-aluminium alloy conductors. Materials and Design, 2006, 27: 821–832.
[11] Khangholi S N, Javidani M, Maltais A, et al. Effects of natural aging and pre-aging on the strength and electrical conductivity in Al-Mg-Si AA6201 conductor alloys. Materials Science and Engineering: A, 2021, 820(14): 1538.
[12] Zheng Y, Bian L P, Ji H L, et al. Influence of Ca and Mn on microstructure, mechanical properties, and electrical conductivity of as-cast and heat-treated Al-Mg-Si alloys. Rare Metal Materials and Engineering, 2022, 51(11): 4010–4020.
[13] Valiev R Z, Murashkin M Y, Sabirov I. A nanostructural design to produce high strength Al alloys with enhanced electrical conductivity. Scripta Materialia, 2014, 76: 13–16.
[14] Pandee P, Gourlay C, Belyakov S, et al. $AlSi_2Sc_2$ intermetallic formation in Al-7Si-0.3Mg-*x*Sc alloys and their effects on as-cast properties. Journal of Alloys and Compounds, 2018, 731: 1159–1170.
[15] Yuan W H, Liang Z Y, Zhang C Y, et al. Effects of La addition on the mechanical properties and thermal-resistant properties of Al-Mg-Si-Zr alloys based on AA 6201. Materials Design, 2012, 34: 788–792.
[16] Zheng Q J, Jiang H X, He J, et al. Effect of micro-alloying La on precipitation behavior, tensile properties and electrical conductivity of Al-Mg-Si alloys. Science China Technological Sciences, 2021, 64(9): 1–11.
[17] Vladislav D, Evgeny P, Pavel S, et al. Effect of La addition on solidification behavior and phase composition of cast Al-Mg-Si alloy. Metals, 2020, 10(12): 1673–1673.
[18] Zhao Y, Zhang Y B, Li T J, et al. Effects of rare earth element La on the microstructure and properties of Al-Mg-Si alloy. Special Casting and Nonferrous Alloys, 2021, 41(10): 1219–1223. (In Chinese)
[19] Medvedev A E, Murashkin M Y, Enikeev N A, et al. Enhancement of mechanical and electrical properties of Al-RE alloys by optimizing rare earth concentration and thermo-mechanical treatment. Journal of Alloys and Compounds, 2018, 745: 696–704.
[20] Jiang H X, Zheng Q J, Song Y, et al. Influence of minor La addition on the solidification, aging behaviors and the tensile properties of Al-Mg-Si alloys. Materials Characterization, 2022, 185: 111750.
[21] Ding W W, Zhao X Y, Chen T L, et al. Effect of rare earth Y and Al-Ti-B master alloy on the microstructure and mechanical properties of 6063 aluminum alloy. Journal of Alloys and Compounds, 2020, 830: 154685.
[22] Jiang H X, Li S X, Zheng Q J, et al. Effect of minor lanthanum on the microstructures, tensile and electrical properties of Al-Fe alloys. Materials & Design, 2020, 195: 108991.
[23] Zheng Q J, Zhang L L, Jiang H X, et al. Effect mechanisms of micro-alloying element La on microstructure and tensile properties of hypoeutectic Al-Si alloys. Journal of Materials Science and Technology, 2020, 47(12): 142–151.
[24] Tsai Y C, Chou C Y, Lee S L, et al. Effect of trace La addition on the microstructures and tensile properties of A356 (Al-7Si-0.35Mg) aluminum alloys. Journal of Alloys and Compounds, 2009, 487: 157–162.
[25] Raghavan V. Al-Fe-La (aluminum-iron-lanthanum). Journal of Phase Equilibria, 2001, 22: 566–567.
[26] Liao H C, Liu Y, Lu C L, et al. Effect of Ce addition on castability, tensile properties and electric conductivity of Al-0.3Si-0.2Mg alloy. International Journal of Cast Metals Research, 2015, 28(4): 213–220.
[27] Shi Z M, Gao K, Shi Y T, et al. Microstructure and tensile properties of rare-earth-modified Al-1Fe binary alloys. Materials Science and Engineering: A, 2015, 632(24): 62–71.
[28] Wang T M, Chen Z N, Fu H W, et al. Grain refinement mechanism of pure aluminum by inoculation with Al-B master alloys. Materials Science and Engineering: A, 2012, 549: 136–143.
[29] Zhou S H, Napolitano R E. Phase equilibria and thermodynamic limits for partitionless crystallization in the Al-La binary system. Acta Materialia, 2006, 54(3): 831–840.
[30] Li S X, Jiang H X, Li Y Q, et al. Influence of rare earth cerium on the microstructures and performances of Al-Fe alloy. Science China Technological Sciences, 2023, 66(11): 3317–3327.
[31] Zheng Q J. Effect of micro-alloying element La on the microstructures and properties of Al-(Mg)-Si alloys. Doctoral Dissertation, Hefei: University of Science and Technology of China, 2021. (In Chinese)
[32] Pan Q L, Li S L, Zou J X, et al. Effcts of minor manganese addition on microstructures and tensile properties of Al-Mg-Si alloys. The Chinese Journal of Nonferrous Metals, 2002, 11(5): 972–976.
[33] Liu H, Liu Y H, Zhao G, et al. Effects of Mn on constituents of Al-Mg-Si-Cu alloys. The Chinese Journal of Nonferrous Metals, 2004, 11: 1906–1911.
[34] Wang D W, Fu Y D, Li T, et al. Role of rare earth elements in wrought aluminum alloys and their development trend. Light Alloy Fabrication Technology, 2020, 48(12): 19–24, 31.
[35] Liang Z Y. Effect of elements addition on microstructure and properties of Al-Mg-Si aluminum alloy used for electrical conductor. Master's Dissertation, Changsha: Hunan University, 2013. (In Chinese)
[36] Hosseinifar M, Malakhov D V. The sequence of intermetallics formation during the solidification of an Al-Mg-Si alloy containing La. Metallurgical and Materials Transactions: A, 2011, 42(3): 825–833.
[37] Li H. Mechanism of La effect on morphology of Al-RE in AZ80-Ce alloy. Master's Dissertation, Chongqing: Chongqing University, 2021. (In Chinese)
[38] Liu S F, Luo L M, Zhou J P, et al. Effect of yttrium addition on as-cast microstructure and properties of 6063 aluminum conductors. Journal of the Chinese Society of Rare Earths, 2018, 36(2): 202–207.
[39] Fu G S, Sun F S, Ren L Y, et al. Modification behavior of trace rare earth on impurity phases in commercial pure aluminum. Chinese Journal of Rare Earths, 2001, 19(2): 133–137.